

A Focal Plane Visual Motion Measurement Sensor

Ralph Etienne-Cummings, *Student Member, IEEE*, Jan Van der Spiegel, *Senior Member, IEEE*, and Paul Mueller

Abstract—A motion detection algorithm, based on biological and computational models, for focal plane implementation has been developed. This Temporal Domain Optical Flow Measurement (TDOFM) algorithm uses computational components which have direct and compact electronic counterparts. It uses a binary image of zero-crossings, 2 level analog signals, the signs of spatiotemporal derivatives, 1-b multiplication and pulsewidths to measure image velocity. Compared to other IC visual motion detectors, this sensor represents the first instance of a robust, wideband and general purpose 2-D motion sensor which reports speed and direction explicitly, has a wide dynamic range and has a compact IC implementation. The front-end of the motion cells is an edge detection circuit which responds to 5–6 orders of magnitude of light intensity and produces near maximum outputs for contrasts as low as 40% in bright and dim ambient conditions. The theoretical velocity measurement dynamic range of the sensor is 4–5 orders of magnitude, and motion ranging over three orders of magnitude has been measured. The variation in the measured speed is less than 15% across 1- and 2-D implementations, multiple chips, cells and directions. The complete system, including the photoreceptors and edge detection circuits, consumes less than 0.4 mW per cell at ± 3.5 V.

Index Terms—Computational sensor, motion chip, visual motion detection.

I. INTRODUCTION

VISUAL MOTION PLAYS a crucial role in understanding of the environment [1]. Using visual motion together with other visual cues, many attributes of the world can be extracted in a robust and unambiguous manner. For example, two objects of the same color and intensity which occlude one another can be perceived as a single object unless they move relative to each other. A wealth of information, which is not easily extracted in static situations, can be obtained from the analysis of dynamic sequences. In particular, visual motion estimation is of fundamental importance in target fixation and tracking, in extracting 3-D structure from motion (especially in the monocular case), in object segmentation, in determining self or ego motion, in avoidance and navigation and in video compression and coding [1]–[4]. Visual motion estimation has been performed primarily in software [4]–[7]. Despite the vast improvements in computer speeds, the measurement of visual motion is still slow (a few frames per second). Hence, image understanding for real-time interaction with the environment is still difficult. However, hardware visual motion detection

does offer an avenue through which the computational overhead associated with dynamic scene analysis can be reduced. In addition, hardware motion detection can be directly used in surveillance systems (motion detection and camera tracking), speed-limit enforcement and slip measurement for automobiles.

Hardware image motion measurement has been attempted through two approaches. The first takes a completely computational direction [8]–[11]. In such approaches, the mathematical techniques which have been developed for software implementations are converted into hardware. This has been largely unsuccessful because it attempts to map computations onto incompatible substrates. A popular approach for image motion measurement, known as the gradient method, depends on highly accurate graded spatiotemporal derivatives, multiplications and divisions. Hence, it is highly susceptible to noise and is unrealizable in compact hardware. The second method of image motion estimation is based completely on biological models, and it has been more successfully implemented than the computationally based model [12]–[15]. The biological models, which use delayed local correlation primarily, are excellent for direction detection, but they do not report speed explicitly, require large circuits and are limited to narrow spatiotemporal bandwidths. Therefore, to develop a general purpose image motion detection technique, an amalgamation of the biological and computational models, which uses the directional selectivity of the biological models and the speed measurement capabilities of the computational models, offers a potentially better technique than these individual models.

This paper presents a visual motion estimation algorithm which adopts the philosophy outlined above. By taking into account the limitations of the IC hardware, a compact and general purpose focal plane image motion detection system, which is implementable directly into analog hardware, is obtained. The algorithm, called the Temporal Domain Optical Flow Measurement (TDOFM) technique, uses the simplicity of biologically based nearest neighbor correlation to detect the direction of motion [16]. Motion is given by the disappearance (–ve temporal derivative) of the zero-crossings from one pixel, AND its reappearance (+ve temporal derivative) at a neighboring pixel. The measurement of the transfer time of the edge at the new pixel gives its speed. Hence, speed is inversely proportional to the time the edge spends at a pixel. Since this algorithm uses a temporal differentiation to detect motion, it has a wider bandwidth than the delayed correlation models. It requires only the signs of the spatiotemporal derivatives and 1-b Boolean multiplications, making it more robust to noise and circuit variation than the gradient approach. This also results in a compact hardware implementation.

Manuscript received September 18, 1995; revised February 8, 1996. This paper was recommended by Associate Editor H. P. Graf.

R. Etienne-Cummings is with the Department of Electrical Engineering, Southern Illinois University, Carbondale, IL 62901 USA.

J. Van der Spiegel is with the Moore School of Electrical Engineering, Center for Sensor Technologies, University of Pennsylvania, Philadelphia, PA 19104 USA.

P. Mueller is with Corticon, Inc., Philadelphia, PA 19104 USA.

Publisher Item Identifier S 1057-7122(97)00892-1.

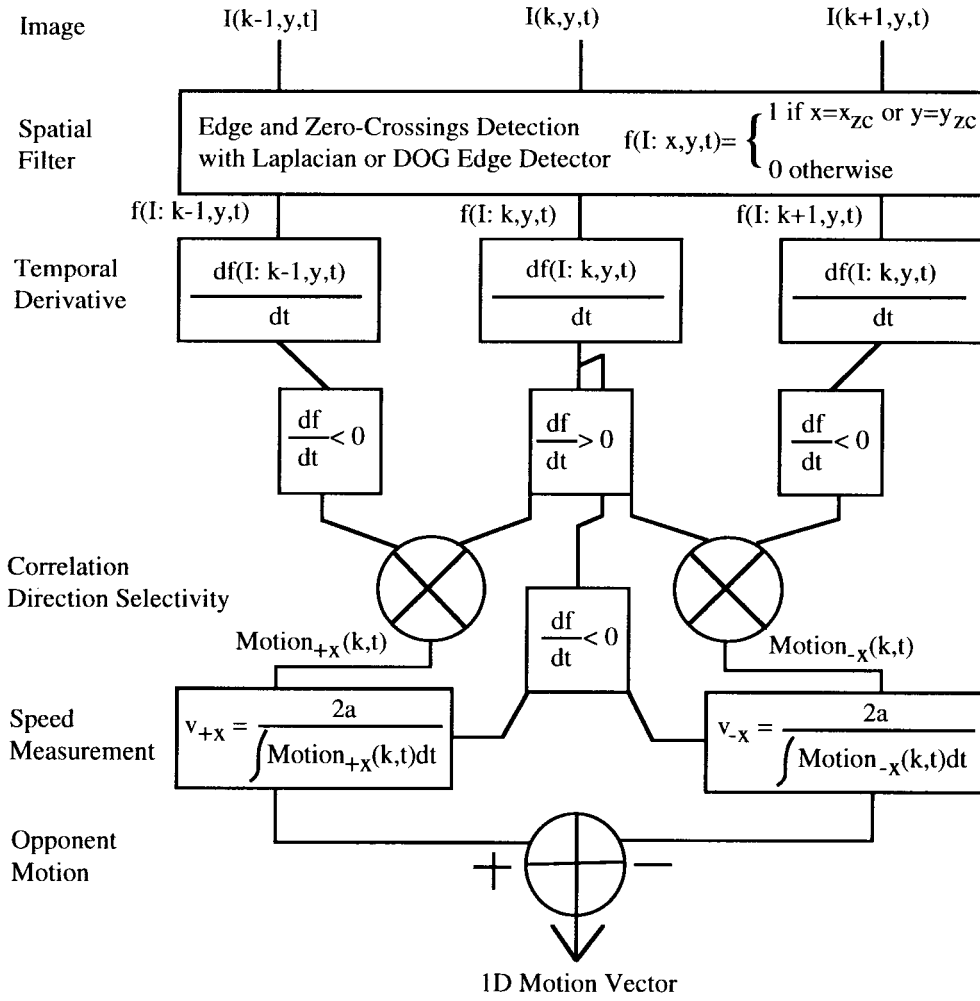


Fig. 1. 1-D system diagram of the TDOFM algorithm.

II. THE TDOFM ALGORITHM

A. Algorithmic Concept

The first step of the TDOFM algorithm is to define what events constitute motion. In the original biological model, proposed by Reichardt, motion is defined by the appearance of light intensity at one pixel followed by its later appearance at a neighboring pixel [16], [17]. This definition is weak and is susceptible to spatial and temporal aliasing [8]. Hence, a stronger definition is used in the TDOFM algorithm: motion is composed of the disappearance of the zero-crossings of image edges at a pixel at its reappearance at a neighboring pixel. The (dis)appearance of the zero-crossing is given by the (negative) positive temporal derivative at the pixel. Hence, motion is detected by AND gating the positive derivative of the zero-crossing of the edge at one pixel with the negative derivative at a neighboring pixel. The direction of motion is given by the neighboring pixel from which the edge disappeared. Provided that motion has been detected at a pixel, the transfer time (pulsewidth) of the edge over the finite geometry of the pixel is inversely proportional to its speed. The motion pulse is integrated and a reciprocal function is computed if required for the application [18]. Fig. 1 shows the computational flow diagram of this approach.

B. Motion Detection with the TDOFM Algorithm

In order to understand the hardware implementation of the motion sensor, the analytical representation of the algorithm for the 1-D case is first presented. Consider an image consisting of a moving bright bar. Let the bright bar extend over m pixels such that it can be represented with (1), where $2a$ is the pixel spacing, $2an$ is the location of the start of the bar and m is its length, as shown in Fig. 2. The edges of the image is next computed

$$I(x, t) = u[x - 2an - v_x t] - u[x - 2a(n + m) - v_x t] \quad (1)$$

with a Laplacian edge detector. The Laplacian is approximated with a three point second order spatial derivative $[-1, 2, -1]$. By approximating the location of the zero-crossings with the positive component of the edge, the zero-crossings are given by (2). Since the pixels have a finite size of $2a$, and assuming that the pixels have short response times (compared to the time spent by each zero-crossing at a pixel), the output of zero-crossing

$$f(I: x, t) = \begin{cases} 1 & \leftarrow \frac{\partial^2}{\partial x^2} I(x, t) > V_z \\ 0 & \leftarrow \frac{\partial^2}{\partial x^2} I(x, t) < V_z \end{cases} \Rightarrow$$

$$f(I: x, t) = \delta[x - 2an - v_x t] + \delta[x - 2a(n + m) - v_x t] \quad (2)$$

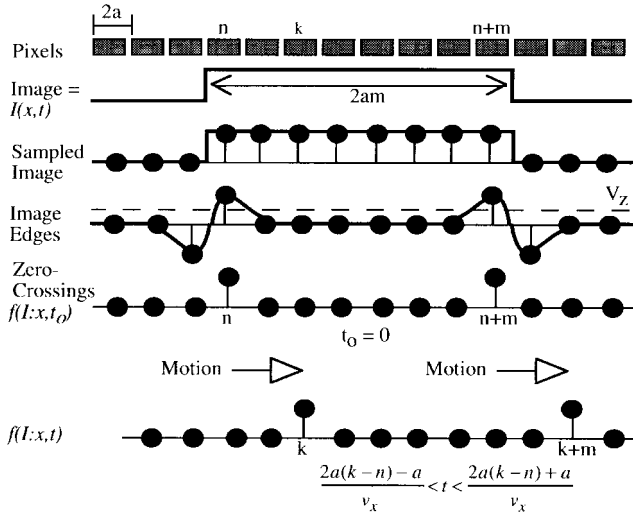


Fig. 2. Imaging, edge detection and zero-crossing identifications processes for a light bar moving to the right.

detection at position $x = 2ak$, where $n < k < n + m$, is given by (3). Equation (3) assumes that the bar is moving in the positive x direction since the edge appears at $x = 2ak - a$ before $x = 2ak + a$. Fig. 2 shows a diagram of the moving bar and the sequence of computations. From (3) the relationship between the transfer time and the speed of the edge is explicit, however, motion must first be detected before this relationship can be exploited.

$$\begin{aligned} \text{arrival: } x &= (2ak - a) @ t_a = \frac{2a(k - n) - a}{v_x}; \\ \text{departure: } x &= (2ak + a) @ t_d = \frac{2a(k - n) + a}{v_x}. \end{aligned} \quad (3)$$

Motion is detected when the arrival (+ve temporal derivative) of the edge at position $2ak$ coincides with its disappearance (−ve temporal derivative) from position $2a(k - 1)$ or $2a(k + 1)$. By substituting $(k - 1)$ and $(k + 1)$ for k in (3), the disappearance times from the two neighboring pixels can be obtained. Equation (4) gives the output of the motion detection correlation. Motion in the x direction is not observed in (4a).

$$\begin{aligned} \text{motion}_{-x} &= \left[\frac{\partial}{\partial t} f(I : 2ak, t) > 0 \right] \\ &\times \left[\frac{\partial}{\partial t} f(I : 2a(k + 1), t) < 0 \right] = 0 \end{aligned} \quad (4a)$$

$$\begin{aligned} \text{motion}_{+x} &= \left[\frac{\partial}{\partial t} f(I : 2a(k - 1), t) < 0 \right] \\ &\times \left[\frac{\partial}{\partial t} f(I : 2ak, t) > 0 \right] \\ &= \delta \left[t - \frac{2a(k - n) - a}{V_x} \right] \delta[x - 2ak]. \end{aligned} \quad (4b)$$

On the other hand, motion in the $+x$ direction is given by a coincidence of negative temporal derivative at $x = 2a(k - 1)$ and positive derivative at $x = 2ak$. This occurs at $t = [2a(k - n) - a]/v_x$. This is consistent with construction of the proof which indicated that the bright edge moved in $+x$ direction. Similarly, the detection of motion in $-x$ direction can be constructed.

To measure the speed of motion, the time interval between the instant of the detection of motion at a pixel, and the disappearance of the edge from that pixel must be determined. Equation (4b) gives the instant at which motion is detected at pixel $2ak$, and (3) gives the time when the edge disappears from the pixel. Hence, speed is given by (5), where t_m and t_d are the times when motion is detected and the edge disappears from pixel $2ak$, respectively. The graphical representation of the motion detection process is illustrated with the “timing” diagram for the various stages of the algorithm shown in Fig. 3.

$$\begin{aligned} \text{Motion: } t_m &= \frac{2a(k - n) - a}{v_x}; \\ \text{Disappear: } t_d &= \frac{2a(k - n) + a}{v_x}; \\ \text{Speed}_{+x} &= \frac{2a}{t_d - t_m} = v_x \end{aligned} \quad (5)$$

III. HARDWARE IMPLEMENTATION

The temporal domain optical flow measurement technique has been developed primarily for hardware implementation. Every component of the computational model has a simple hardware counterpart. Chips containing linear (1×9) and 2-D (5×5) arrays of motion detecting pixels have been fabricated in $2 \mu\text{m}$ CMOS through MOSIS. This section outlines the circuits used to realize the chips.

The first three layers of focal plane processing are considered as the front-end of the motion detection algorithm. They consist of phototransistors for light transduction, logarithmic compression to span a large operating range of light intensity and edge detection to realize the zero-crossing detectors. The edge detection circuit is implemented with a passive resistive array, which approximates a Laplacian edge detector with a difference-of-Gaussian operator [18]–[20]. The edge detection process is obtained by subtracting a smoothed, via the resistive grid, version of an image from the original image. The output of the edge detector is the input to the motion detection system.

A. Zero-Crossing Detection

The analog outputs of the edge detection circuit are converted into binary signals at the locations of the zero-crossings by using a comparator. The threshold level of the comparator is set based on the expected signal to noise ratio of the image. Since the edge detectors are designed with high contrast sensitivities, the typical threshold level is 20% of full-scale. The comparator is implemented with hysteresis to prevent oscillations due to noise and slow varying edges for slow motion. Thresholding the edges provides an approximate image of the zero-crossings, normalizes all the discontinuities to a single value, and also removes some weak spurious edges due to noise. Furthermore, by using a CMOS inverter output stage, the fast switch time of the zero-crossing detector results in smaller component sizes in the temporal differentiator circuit.

The comparator implementing the zero-crossing detection circuits is the first stage of the motion detection circuit. Fig. 4 shows a schematic for transforming the computational flow diagram in Fig. 2 into CMOS circuitry. This schematic shows

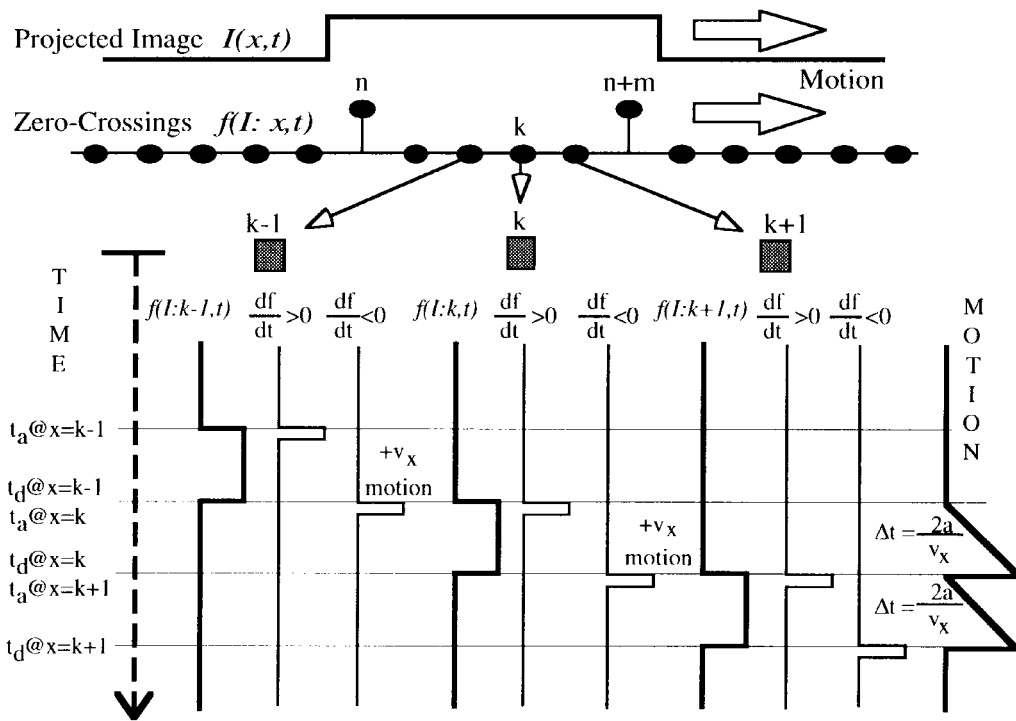


Fig. 3. Motion detection timing diagram for a bright bar moving to the right.

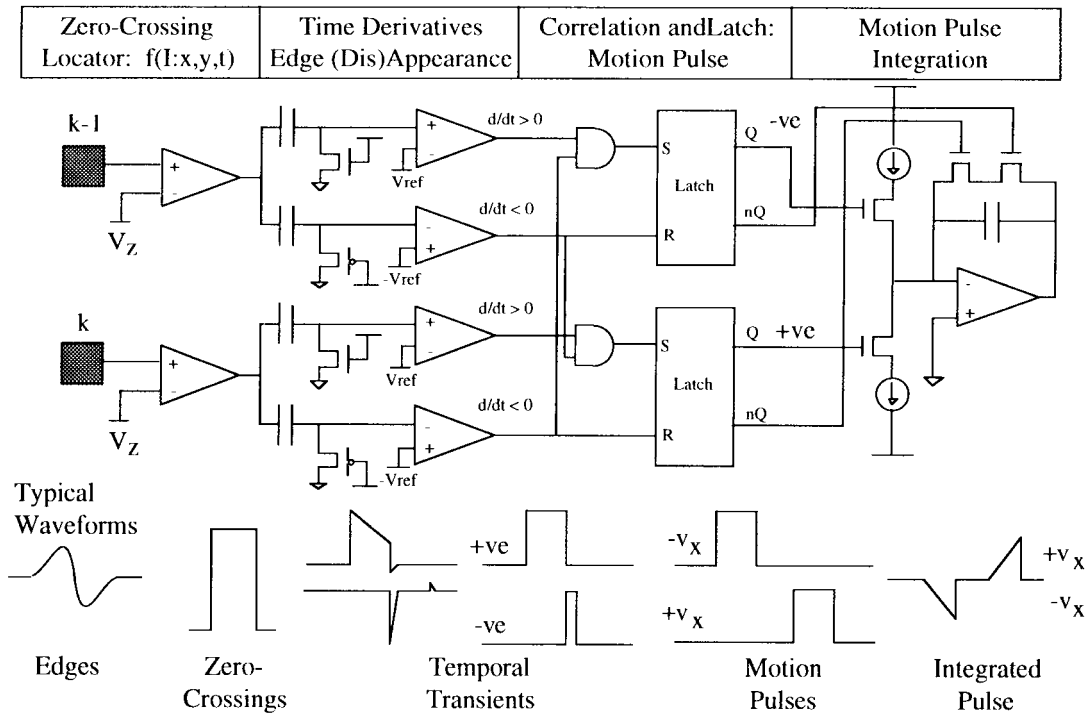


Fig. 4. Schematic of the motion detection circuit, whose input is provided edge detection circuit.

two halves of a cell of a 1-D motion detection circuit from two adjacent pixels. In the 2-D array, the same circuit is also used in the two orthogonal directions.

B. The Appearance and Disappearance Detectors: Temporal Differentiators

The simplest circuit to approximate a temporal differentiator is an RC transient detection circuit, as shown in Fig. 4. An

RC transient detector outputs a large, but decaying, voltage at a rising or falling temporal transition in its input due to capacitive coupling. Since two transient detectors are required at each pixel, each circuit must occupy a small area. Using a PMOS transistor where the source, drain and bulk are tied together as one plate and the gate as the other plate of the floating capacitor, the maximum capacitance per unit area, C_{ox} , can be obtained. The voltage dependent capacitance

and nwell depletion parasitic capacitance do not degrade the performance of the transient detectors. However, this type of capacitor is light sensitivity and must be well shielded.

To minimize the area of the transient detectors, small capacitors and small discharge currents are used. The discharge time of the transient detectors must be hundreds of milliseconds for slow-moving edges. The small PMOS capacitors require discharge currents of tenths of nanoamps to realize these large discharge times. These discharge currents are easily implemented with off-chip biasing. Furthermore, the off-chip biasing makes the discharge time controllable. However, the discharge transistors are also sensitive to light and must be shielded when implemented at the focal plane.

Using the current source to realize the discharge time of the transient detectors has some pros and cons. The immediate benefits are its compactness, ease of implementation and controllability. One disadvantage is by using an NMOS (PMOS) transistor, the transient detector will have the prescribed discharge time for the rise (fall) of the input signal, but much shorter in the opposite transition. The difference in the discharge currents is caused by the bidirectionality of MOS transistors, since the location of drain and source changes depending on the direction of current flow. The repercussion of this asymmetry is that two independent transient detectors must be used per pixel, although a single capacitor circuit is possible if the NMOS and PMOS transistors are connected in series. In the former case, one circuit is used to detect rising edges, while the other detects falling edges, as can be seen in Fig. 4. The area penalty is obvious, but there is a benefit in that each circuit readies itself quickly in the face of the opposite polarity transients. Furthermore, there is no coupling between the two circuits which means that they are both free to output their maximum voltage, independent of what previous input transients were present. When the NMOS and PMOS current sources are connected in series, the negative (positive) swing is limited if the rise (fall) to fall (rise) time interval is much shorter than the discharge time.

The appearance and disappearance of edges at a pixel are given by the polarity of the temporal transitions of the zero-crossings, where a rise corresponds to appearance while a fall indicates disappearance. Comparators are used with the two transient detectors to provide binary signals to the correlators (see Fig. 4). Hence, only the sign of the temporal differentials, and not graded values, are used to detect motion. This allows the circuits to be simple, compact and less prone to inaccuracies due to process variations.

C. The Correlators

The correlators are implemented with simple AND gates, whose inputs are the differentiators' outputs. Motion is detected by correlating (AND function) the appearance of an edge at a pixel with its disappearance from a neighboring pixel. Four such correlators are used at each pixel to determine from which of the neighbors the edge disappeared, and thus, extract 2-D direction. The discharge time of the transient detectors allows the correlation to be obtained even when the disappearance from one pixel and the appearance at a neighboring pixel is not

simultaneous. The discharge time of the appearance detector is designed to be larger than the disappearance detector since the edge detection circuit causes the edge to appear at a pixel before it completely disappears from a previous pixel. Since all the signals in the motion detection circuit are binary, the correlation can easily, compactly and robustly be computed with AND gates.

D. The Speed Detector

Speed is extracted by measuring the time interval between the detection of motion and the disappearance of the edge from the pixel. Since the output of the correlator is binary, a flip-flop latch is used to measure the time interval. When motion is detected, the output of the correlator sets the latch to a high state. The latch remains high until a negative transient, edge disappearance, is detected. Hence, the pulsewidth of the latch is inversely proportional to the speed of the moving edge. Using the latch to produce the motion pulse has vital advantages over using the correlator output itself. The latch allows extremely slow speeds to be detected, even if the discharge times of the transient detectors are shorter than the time spent at a pixel. The only requirement is that the correlation must be made. An additional advantage of using the latches is that the discharge time of the negative transient detectors can be made as short as possible. A short negative differential pulse helps reduce temporal aliasing for stimuli moving very fast or having high spatial frequencies. Fig. 4 shows the location of the latches in the motion detection circuits. There are four such latches per pixel for the 2-D array of motion detectors.

E. Opponent Motion and Pulse Integration

The output of the four latches provides the motion pulses for the two orthogonal motion. Depending on the intended use of the measured velocity, the two motion pulses from each direction can be combined such that a single bipolar signal is used to represent each of the motion components. Fig. 4 shows the circuit for the 1-D case. The outputs of the latches for the two opposite directions of motion are used to activate two current sources of opposite polarities. The currents are fed into an integrator, whose output is then proportional to the pulsewidths, while the polarity of the integrated signal gives the direction of motion. In this scheme, the two current sources must be matched such that equal motion pulses in opposite directions will produce equal but opposite integrated voltages. Furthermore, the current sources can be externally controlled to set the rate of integration. Moreover, the current sources can be biased output small currents such that a small integration capacitor can be used.

Depending on the intended use of the measured motion, a reciprocal circuit can be used to obtain a signal which is directly proportional to speed [21]. In other applications, the integrated voltages or the motion pulses may be sufficient. Clearly, there are area penalties for the inclusion of the additional circuits per pixel. In addition, using an opamp to implement the integrator consumes large areas, which indicates that other more compact circuits must be used.

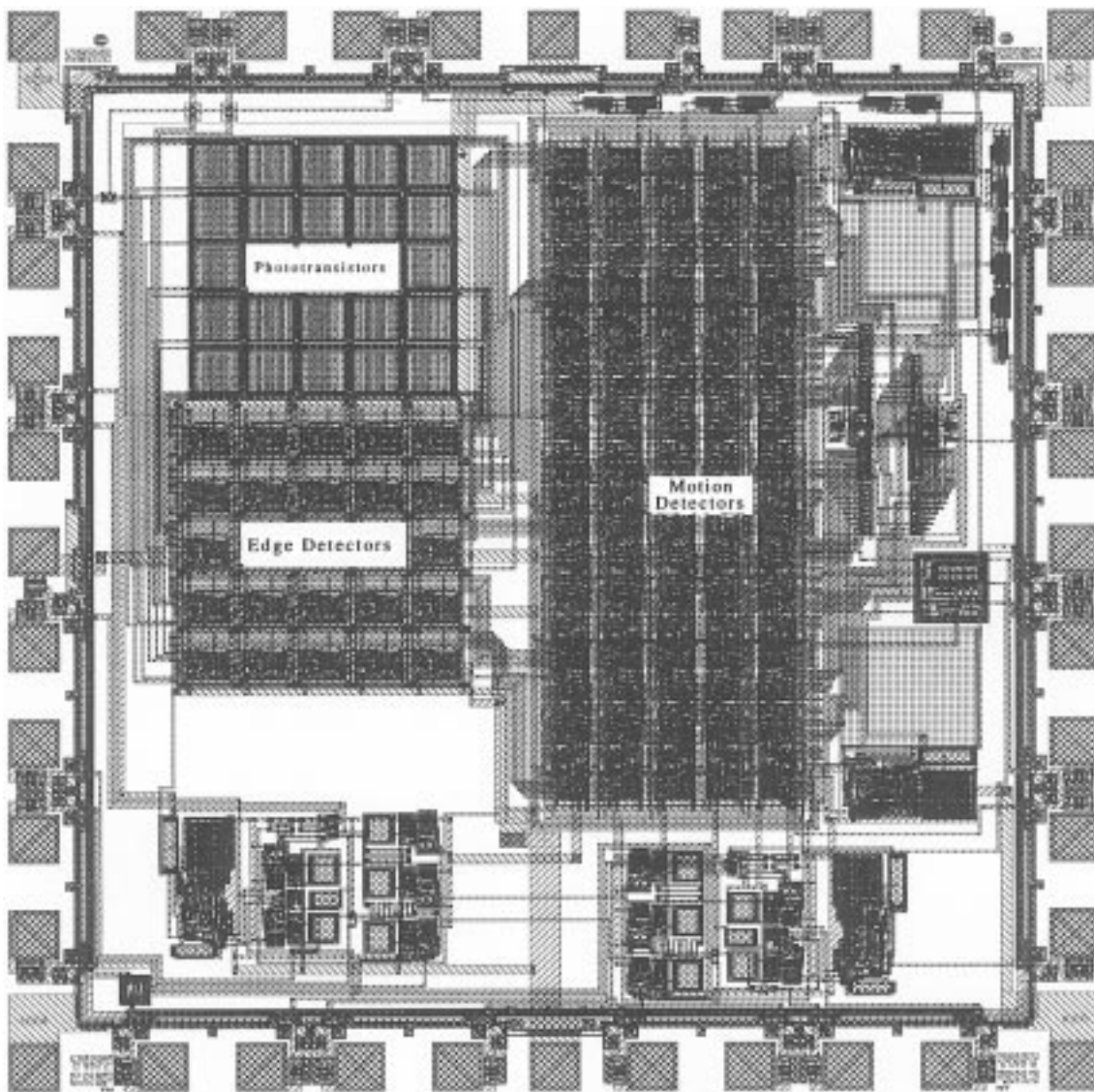


Fig. 5. Layout of the 2-D motion detection chip: 5×5 arrays of motion detectors.

IV. EXPERIMENTAL RESULTS

Chips containing 1- and 2-D arrays of the motion detectors have been implemented in $2\ \mu\text{m}$ Nwell CMOS through the MOSIS foundry. Table I summarizes the characteristics of the front-end circuitry, i.e., the phototransduction, logarithmic compression and edge detection. The cell size listed in the table combines the phototransistor and the edge detection circuits even though they are laid-out physically apart as shown in the Fig. 5. The response time of the edge detection circuit, which is given in Table II, is ambient intensity dependent due to the large on-resistance of diode-connected transistors for small drain currents (low light). However, the chips are designed to operate in indoor ($25\ \mu\text{Wcm}^{-2}$) to outdoor light ($250\ \mu\text{Wcm}^{-2}$). Hence, under normal operating conditions, the shortest motion pulses, which are defined to be 10 times the rise time + fall time, are 400 and 125 μs in room light and sun light, respectively. During the testing of the motion detection circuits, bright and dark lines are projected onto the chip while the ambient intensity is varied. Hence, the quantitative results presented correspond to these stimuli of various contrasts.

Two important circuit design issues affect the performance of the motion detection circuits. The zero-crossing comparators must be implemented with hysteresis to eliminate “bouncing” in the comparator output when the edge detector outputs oscillate about the threshold level due to noise. The “bounces” in the comparator outputs trigger false appearances and disappearances, such that erroneous motion is recorded. These oscillations become more apparent for slow edges since the output of the edge detector varies at a much slower rate and therefore stays close to the threshold level for an extended period of time. Second, using two independent transient detectors as shown in Fig. 4 results in more robust motion detection than using a single bidirectional circuit. Despite the larger circuit area of the former approach, it is responsive to a wider range of motion and less susceptible to complementary transistor mismatch and intercell variations. These two factors are incorporated into the circuits used to implement the motion sensor.

Fig. 6 shows the oscilloscope traces of the various computational stages of two adjacent motion detection cells for a

TABLE I
CHARACTERISTICS OF THE PHOTORECEPTORS, LOGARITHMIC
COMPRESSION AND EDGE DETECTION CIRCUITS

Technology	2 μm Nwell (ORBIT)
Chip Size	2.3 x 2.3 mm ²
Package	40 Pin DIP
No. of Pixels	1 x 9 and 5 x 5
Photoreceptor Size	100 x 100 μm^2
Cell Size	110 x 220 μm^2
Fill Factor (+ Edge Detectors)	41%
Operating Intensity Range	3 nWcm ⁻² to 2 mWcm ⁻²
R1 (Resistive Grid)	70 K Ω (Nwell)
R2 (Feedback)	200 K Ω (PMOS)
Opamp Gain	77
Opamp BW	1.2 MHz
Output Swing	1.5 to -2.5 V
Power	0.35 mW/cell @ +/- 3.5 V

TABLE II
PERFORMANCE LIMITATIONS OF THE MOTION SENSOR

Ambient Intensity	2.5 μWcm^{-2} Low Room Light	25 μWcm^{-2} Normal Room Light	250 μWcm^{-2} Sun Light
Edge Detectors	RT < 60 μs FT < 100 μs	RT < 10 μs FT < 30 μs	RT < 2.5 μs FT < 10 μs
Motion Detection Maximum	PW: 1.6 ms Speed: 7.1 cm/s	PW: 400 ms Speed: 28.9 cm/s	PW: 125 ms Speed: 92.9 cm/s
Motion Detection Minimum	PW: 2.5 s Speed 0.04 mm/s	PW: 2.5 s Speed 0.04 mm/s	PW: 2.5 s Speed 0.04 mm/s
Integrated Pulse	Minimum: 30 mV Maximum: 3V	Speed Range: 2 Orders of Magnitude $V_{\text{out}} = 0.03[V_{\text{el}_{\text{max}}}/V_{\text{el}}]$	

bright edge moving to the right with an on-chip speed of 8.7 mm/s (44 pixels/s). The top and fourth trace show the output of the edge detector circuits at pixel $k - 1$ and k . Since the edge detection circuit has a better negative swing than positive swing, the zero-crossing detectors are set to trigger on the negative portion of the edge, allowing the threshold to be set relatively high above the noise and random offsets envelop. The edge appears at the neighboring pixel before it leaves the previous pixel. To accommodate this overlap, discharge time for the positive transient detector is long, as seen in the second and fifth traces. The negative transient detectors, shown in the third and sixth traces, have short discharge times. This limits, but does not eliminate, temporal aliasing by quickly resetting the negative transient detectors. Hence, the next edge can appear at the neighboring pixel in short succession without triggering false motion. The last trace shows the output of the motion latch at pixel k . The latch is set at the time when the negative transient (disappearance) at pixel $k - 1$ overlaps with the positive transient (appearance) at pixel k , corresponding to rightward motion. The extent of the overlap between the zero-crossings at the neighboring pixels is also inversely proportional to the edge's speed, which implies that the motion pulsewidth has the correct relationship to speed.

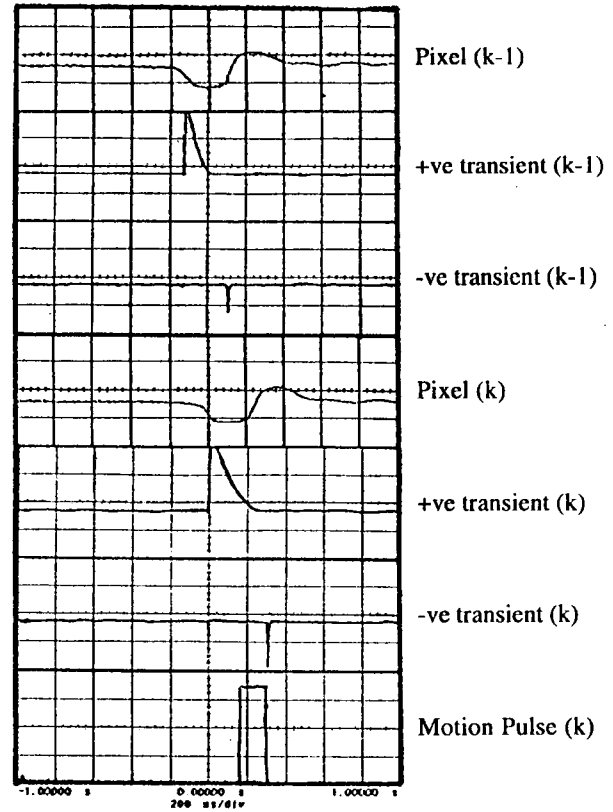


Fig. 6. Measured waveform for various stages of the motion detection process for 2 neighboring pixels as an edge moves to the right. [X-axis: 200 ns/Div].

Fig. 7 illustrates the latter observation and shows the outputs for a fast edge, 0.52 m/s (2600 pixels/s), moving to the right and a slow edge, 2.8 mm/s (14 pixels/s), moving to the left. Fig. 8 shows the output of the edge detectors and the left motion latch for complex images such as a hand moving back and forth. The four fingers are projected onto the chip as a thin dark lines. There is an output every other pass of the hand across the sensor, as expected. Since these motion sensors are intended for a target tracking system, the latch outputs at all pixels are combined to produce a single motion pulse train for each direction. However, the interpulse interval is so short (approximately 3 μs) that the individual pulses are only visible at the output of the integrator. Fig. 9 shows the traces of the motion pulses and the corresponding integrator output. Each pulse is integrated to produce a voltage which is inversely proportional to the speed. Using a reciprocal circuit [21], a voltage can be obtained which is directly proportional to speed. The summary of the measured motion from 1-D (1 x 9) and 2-D (5 x 5) chips are plotted in Figs. 10 and 11, respectively. In the figures, one-over the average measured motion pulsewidth is plotted against on-chip speed ($[Z/z_0] \times \text{Speed}_{\text{on-chip}} = \text{Speed}_{\text{world}}$, where Z is the target distance and z_0 (1.3 cm) is the chip distance from the lens). The reciprocal of the pulsewidth is expected to be linear with stimulus motion, and this is observed (subject to analog variations). Figs. 10(b) and 11(b) show the dynamic range and the variations of the measured motion for the two implementations, multiple chips, multiple pixels, multiple directions. The variations are

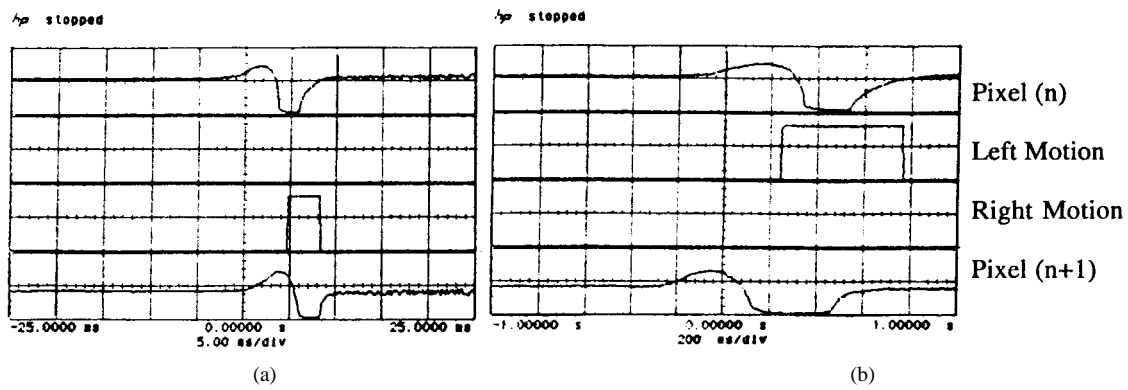


Fig. 7. Measured waveforms of the edge and motion detection for fast (a) and slow (b) motion to the right and left, respectively. [(a) X-axis: 5 ms/Div, (b) X-axis: 200 ms/Div].

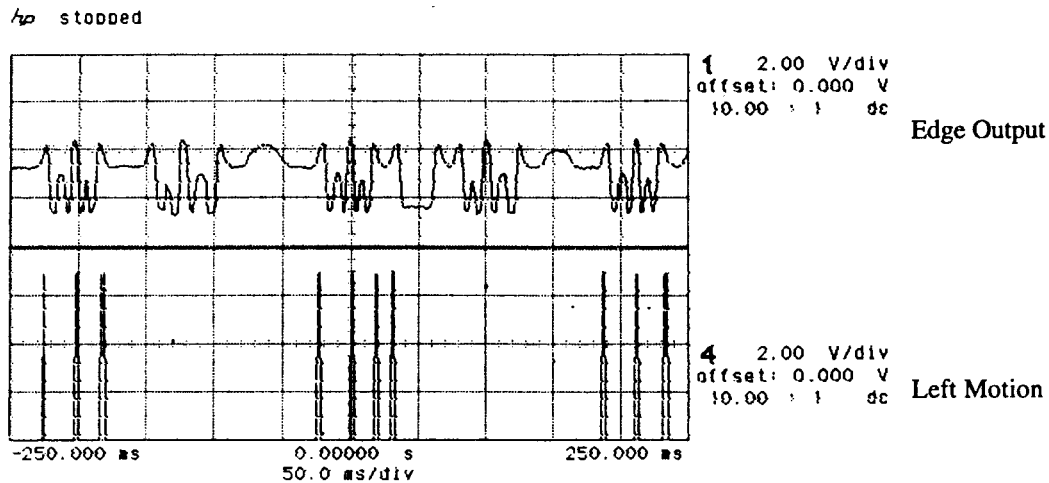


Fig. 8. Measured waveforms of the edge and left motion detection for a hand moving back and forth. Each digit is seen as a thin dark line. [X-axis: 50 ms/Div].

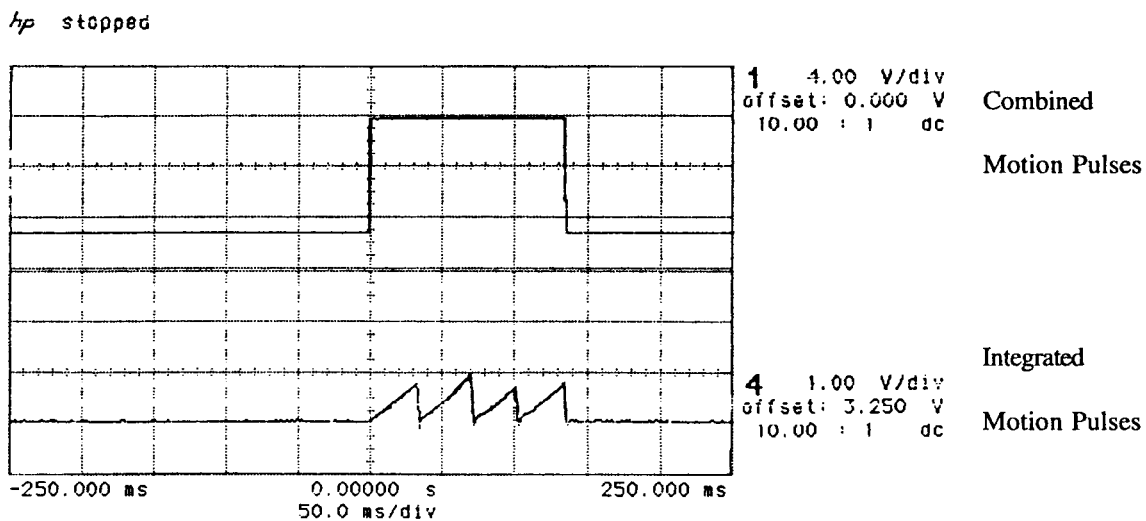
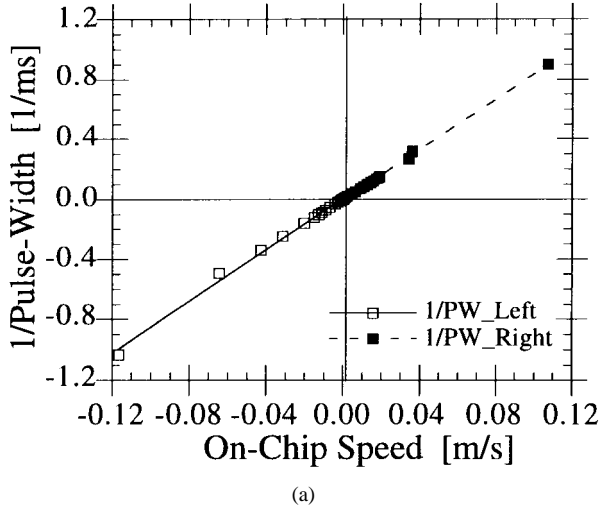


Fig. 9. Measured waveforms of the combined motion pulses (top) and the integrator outputs (bottom) for a moving line. Evidence of the individual pulses are only visible at the integrator output. [X-axis: 50 ms/Div].

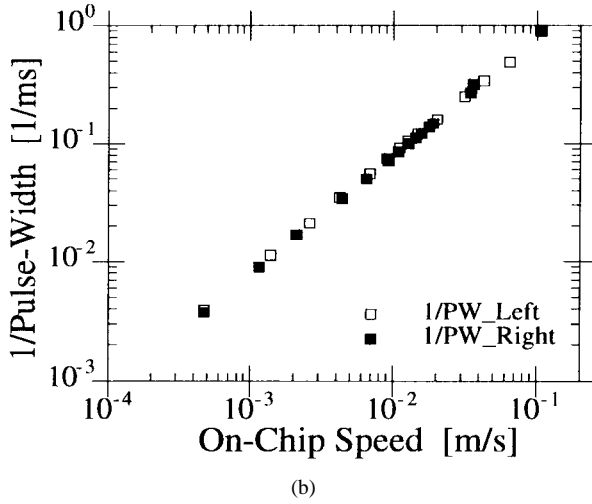
within 15%, and motion is measured ranging over 3 orders of magnitude for edges of contrast ranging from 20 to 100% in bright and dim ambient lighting.

Table III compares our motion chips to other published fully integrated chips. When local correlation is used for direction

selectivity and temporal derivative is used to measure speed, velocity can be measured compactly spanning a wide range [25]. Other correlation approaches either consume much area, and/or they do not report explicit velocity. Explicit velocity is reported when the output (voltage, current, charge, or



(a)



(b)

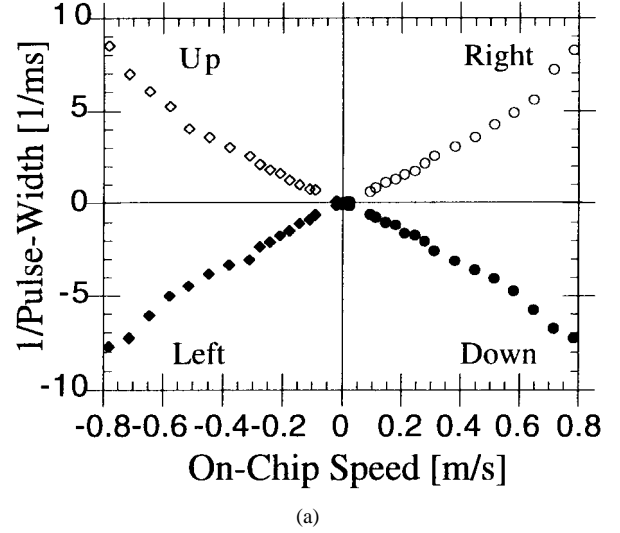
Fig. 10. Measured 1-D motion pulsewidth versus on-chip speed. The average pulsewidths are plotted in (a) and (b) shows the matching between left and right motion cells.

pulsewidth) of the sensors vary monotonically with target speed and direction. In some of the listed chips, the same output is observed for two different target velocities, and requires an additional computational stage to extract the correct value [10], [12], [14], [26]. The gradient based approaches, which can report explicit velocity, usually occupy large areas and are susceptible to noise and component mismatch [9]. The last group of chips do not detect movement, but simply measures the change in pixel intensity over time [23], [24], [27]. This is realized with both discrete and continuous time differentiation. Hence, these chips do not report speed nor direction. The hardware presented in this paper offers compact, 1- and 2-D velocity detection spanning 3–4 orders of magnitude, using a correlative/derivative hybrid approach.

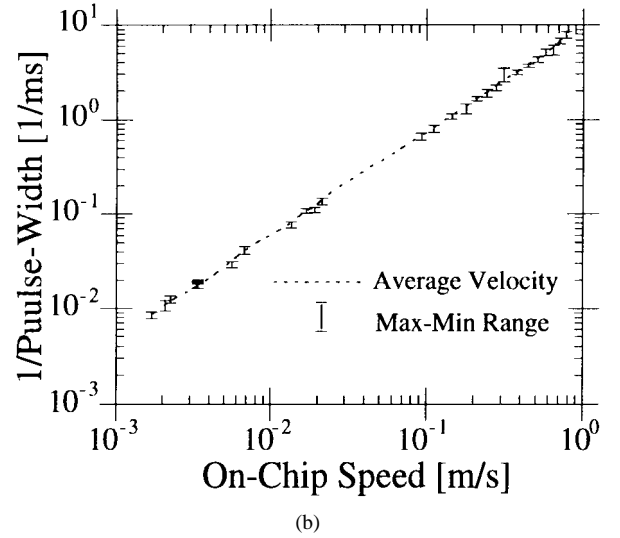
V. LIMITATIONS

A. Spatial Resolution

The spatial resolution of the motion detection chips determines the highest image frequency which the chips can handle



(a)



(b)

Fig. 11. Measured 2-D motion pulsewidth versus on-chip speed. The average pulsewidth is plotted in (a) and (b) shows the deviation (error bars) among direction, cells and chips.

without spatial aliasing. The photoreceptors used in the chips reported are large ($100 \times 100 \mu\text{m}^2$) to increase the sensing fill factor. However, in more practical arrays, i.e., larger than 100×100 pixels, the size of the receptors must be reduced. The interphotoreceptor spacing in the two chips is $10 \mu\text{m}$ since they are laid-out away from the processing circuitry. The size plus spacing of the photoreceptors, $110 \mu\text{m}$, mandate a maximum allowed on-chip spatial frequency of 4.5 cycles/mm. By taking into account the distance of the target from the retina (Z), the relationship between the highest allowed spatial frequency and the target distance is $\nu_{\text{max}} = 4.5(z_0/Z)$, where z_0 is the distance between the lens and focal plane.

B. Contrast Sensitivity

The contrast sensitivity of the motion chips is controlled by the logarithmic and edge detection circuits. Contrast is defined as the ratio of the difference to the sum of the intensity about a discontinuity, i.e., $(I_1 - I_2)/(I_1 + I_2)$. Fig. 12 shows a

TABLE III
COMPARISON WITH OTHER FULLY INTEGRATED MOTION CHIPS

Author	Technique	Array Size	Compact	Explicit Velocity	Speed [Pixels/s]
Etienne-Cummings	Correlative/Derivative	1 x 9, 5 x 5	Yes	Yes	0.36 - 8445
Kramer [25]	Correlative/Derivative	1D	Yes	Yes	8 - 190
Andreou [12]	Correlative	1 x 50	Yes	No	NA
Delbruck [26]	Correlative	26 x 26	Yes	No	NA
Gottardi [22]	Correlative	30 x 1	No	Yes	0 - 3000
Hariuchi [9]	Correlative	1 x 28	No	Yes	50 - 1150
Sarpeshkar [14]	Correlative	1D	Yes	No	NA
Hariuchi [9]	Gradient	1 x 30	No	Yes	10 - 250
Tanner [10]	Gradient	8 x 8	Yes	No	NA
Simoni [23]	Frame Difference	64 x 64	Yes	No	NA
Chong [27]	Temporal Derivative	25 x 25	Yes	No	NA
Wu [24]	Temporal Derivative	32 x 32	Yes	No	NA

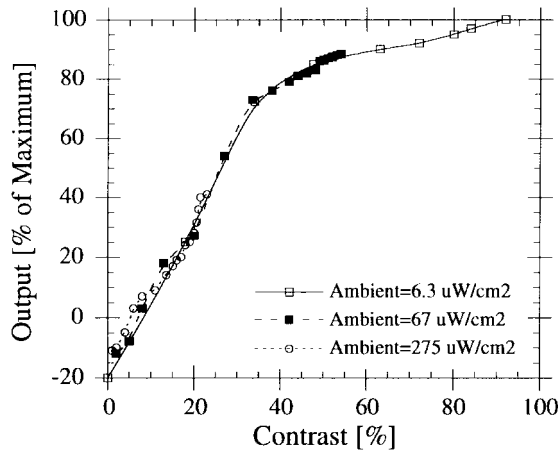


Fig. 12. The contrast sensitivity function of the edge detection circuit.

plot of the measured contrast sensitivity function. The contrast sensitivity function is computed for three ambient conditions. The motion detection circuit, which uses the output of the edge detection circuit, can operate with a minimum signal of ± 0.4 V (minimum required to overcome random offsets in the outputs of the edge detection circuits) which is equal to 20% of the full-scale for the edge detection circuit. The plot indicates that a minimum contrast of 20% is required for the operation of the motion detection system.

C. Maximum and Minimum Target Speed

The maximum target speed that can be measured by the sensor, is determined by the response time of the edge detection circuit. The minimum target speed, on the other hand, is limited by the discharge rate of the transient detectors. The temporal response of the edge detection circuit is ambient intensity dependent. Table II shows a list of the response time

(the sum of the rise and fall times) of the edge detection circuit under various ambient lighting conditions. Since the motion detection circuit measures the pulsewidth of the edge detection circuit, the criterion for the minimum allowed pulse width is taken to be 10 times the response time. Hence, the maximum measurable on-chip speeds are also listed in the table. Even under low light conditions, $2.5 \mu\text{Wcm}^{-2}$, the maximum on-chip speed is still fast enough to capture a target moving at 7 m/s at 1.3 m from the sensor.

The discharge time of the transient detectors determines the minimum speed of the sensor. The discharge time is controlled by off-chip biasing. To ensure the correct performance of the motion detection circuit, the maximum discharge time of the positive transient detector is 400 ms. For larger discharge time, the motion detection circuit suffers from temporal aliasing for fast moving target since the transient detector does not reset quickly. The discharge time of 400 ms allows motion pulses lasting 2.5 s to be measured. Hence, a minimum on-chip speed of approximately 0.04 mm/s is detectable with the motion detection circuits. This speed is too small to be directly measured, and it is determined by the extrapolation of Figs. 10(a) and 11(a).

While the theoretical maximum range of the motion detection circuit, up to the latches, is 4–5 orders of magnitude, the inclusion of the integrator limits the dynamic range to approximately 2 orders. This limitation is largely due to the noise floor. Power supplies and circuits with better noise immunity can improve the dynamic range of the integration stage. However, in some applications of the sensor, the latches can be used as the output stage. In others, further processing such as integrating the pulsewidth and computing a reciprocal function can be performed. Naturally, the additional processing increases the size of the sensor and may reduce its dynamic range.

D. Scalability of the Array

In the current method of implementation, the motion detection array can not be easily scaled to larger sizes due to the interconnection required. Since the photoreceptors are placed away from the edge detectors, which are in turn away from the motion detection array, $2N^2$ wires, where N^2 is the number of pixels, must be routed between the three sections of the chip. Furthermore, the size of the motion detection circuits greatly decreases the number of pixels which can be implemented on a single chip. To circumvent these problems, a multichip approach using a mixture of serial and parallel processing can be taken. An imaging chip containing a dense array of photoreceptors, can be used to sequentially compute the zero-crossings of the image. Groups of pixels, subarrays, can be read-out in parallel, while the individual pixels in the subarrays are read-out serially. This approach will increase the frame rate of the imaging chip, increase the density of the photoreceptors and improve matching by using one zero-crossing detector per subarray. Furthermore, the fill factor of the array can be increased by using small feature and micro-lens technologies. Following the imaging chip, motion detection chip(s) can be used. These chips will demultiplex the image of zero-crossings

and compute motion. The number of lines interconnecting the imaging chip and the motion chips will be $N^2/(\text{number of subarrays})$. Hence, this motion detection technique will be scaleable to larger arrays.

VI. CONCLUSION

A motion detection algorithm for focal plane implementation has been developed. The algorithm is an amalgamation of biologically and computationally based models. It is directly implementable in analog circuits because the limitations of the IC hardware have been considered during the development of the technique. Analysis shows that temporal domain motion detection is obtained.

The algorithm has also been implemented in $2\ \mu\text{m}$ CMOS. The analog hardware realization uses a binary image of zero-crossings, two level analog signals, the signs of spatiotemporal derivatives, 1 b multiplication and pulswidths to measure image velocity. Compared to other integrated visual motion detectors, this sensor represents the first instance of a wide-band focal plane general purpose real-time 2-D visual motion detection sensor which reports speed and direction explicitly, has a wide dynamic range and is compactly, efficiently and robustly implementable in IC technology.

Arrays of 1×9 and 5×5 motion detection cells have been implemented. The front-end of the motion cells is an edge detection circuit which responds to 5–6 orders of magnitude of light intensity and the produces near maximum outputs for contrasts as low as 40%. The motion detection circuit have been measured to operate over 3 orders of magnitude of on-chip speed, and the theoretical limitation is 4–5 orders from 0.04 to 929 mm/s (0.36 to 8445 pixels/s). The maximum speed is dependent on the ambient intensity due to the intensity dependent response time of the edge detector circuit. The maximum speeds are 71, 289, and 929 mm/s in 2.5 (dim indoor), 25 (normal indoor) and 250 (outdoor) μWcm^{-2} light intensity, respectively. The variation in the measured speed is less 15% across the two implementations, multiple chips, cells and directions. The motion detection circuits operate robustly when comparators with hysteresis are used to compute the zero-crossings, and the temporal differentiators are implemented with 2 independent transient detector circuits controlled off-chip. The complete system, i.e., including the photoreceptors and edge detection circuits, consumes less than 0.4 mW per cell.

There are many applications of visual motion in general scene analysis. This motion detection approach can be expanded, using a multichip system, to more practical sizes (128×128 pixels or larger) and used as a front end of many computer vision, robotics and video coding algorithms. In the current form, it can be used in security surveillance as a movement detector. It can also be used as a passive velocity sensor in the law enforcement and automotive industry to complement the speedometer system. In the latter case, it can be used with antilock braking technology to measure skid velocity after the wheels have locked. This motion detection sensor is also applicable to velocity based visual target tracking for military and civilian uses.

REFERENCES

- [1] K. Nakayama, "Biological image motion processing: A review," *Vision Res.*, vol. 25, no. 5, pp. 625–660, 1985.
- [2] L. Spillmann and J. Werner, *Visual Perception*. New York: Academic, 1990.
- [3] M. Landy, B. Doshier, G. Sperling, and M. Perkins, "The kinetic depth effect and optic flow: First and second order motion," *Vision Res.*, vol. 31, no. 5, pp. 859–876, 1991.
- [4] B. Horn, *Robot Vision*. Cambridge, MA: MIT Press, 1986.
- [5] P. Anandan, "A computational framework and an algorithm for the measurement of visual motion," *Int. J. Computer Vision*, vol. 2, pp. 283–310, 1989.
- [6] E. Adelson and J. Bergen, "Spatiotemporal energy models for the perception of motion," *J. Opt. Soc. Amer.*, vol. 2, no. 2, pp. 284–299, 1985.
- [7] E. Hildreth, "The computation of the velocity field," in *Proc. Royal Soc. London B*, 1984, vol. 221, pp. 189–220.
- [8] C. Koch, "Implementing early vision algorithms in analog hardware: An overview," *SPIE, Visual Information Processing: From Neurons to Chips*, vol. 1473, pp. 2–15, 1991.
- [9] T. Horiuchi, W. Bair, B. Bishofberger, A. Moore, C. Koch, and J. Lazzaro, "Computing motion using analog VLSI vision chips: An experimental comparison among different approaches," *Int. J. Computer Vision*, vol. 8, pp. 203–216, 1992.
- [10] J. Tanner and C. Mead, "An integrated optical motion sensor," in *VLSI Signal Processing II*, S.-Y. Kung, R. Owen, and J. Nash, Eds. New York: IEEE Press, 1986, pp. 59–76.
- [11] J. Hutchinson, C. Koch, J. Luo, and C. Mead, "Computing motion using analog and binary resistive networks," *IEEE Trans. Comput.*, vol. 21, pp. 52–64, 1988.
- [12] A. Andreou and K. Strohbehn, "Analog VLSI implementation of Hassenstein-Reichardt-Poggio models for vision computation," in *Proc. 1990 IEEE Symp. Syst., Man Cybern.*, 1990, pp. 707–710.
- [13] R. Benson and T. Delbruck, "Direction selective silicon retina that uses null inhibition," in *Advances in Neural Information Processing Systems*, J. Moody, S. Hanson, and R. Lippmann, Eds. San Mateo, CA: Morgan Kaufmann, 1992, vol. 4, pp. 756–763.
- [14] R. Sarpeshkar, W. Bair, and C. Koch, "An analog VLSI chip for local velocity estimation based on Reichardt's motion algorithm," in *Advances in Neural Information Processing Systems*, S. Hanson, J. Cowan, and L. Giles, Eds. San Mateo, CA: Morgan Kaufmann, vol. 5, 1993.
- [15] R. Etienne-Cummings, C. Donham, J. Van der Spiegel, and P. Mueller, "Spatiotemporal computation with a general purpose analog neural computer: Real-time visual motion estimation," in *Proc. IEEE Int. Conf. Neural Networks*, 1994, pp. 1835–1840.
- [16] W. Reichardt, "Autocorrelation: A principle for the evaluation sensory information by the central nervous system," *Sensory Communication*. New York: Wiley, 1961.
- [17] J. van Santen and G. Sperling, "Temporal covariance model of human motion perception," *J. Opt. Soc. Amer.*, vol. 1, no. 5, pp. 451–473, 1984.
- [18] R. Etienne-Cummings, "Biologically motivated analog VLSI systems for optomotor tasks," Ph.D. dissertation, Dep. Elect. Eng., Univ. Pennsylvania, Philadelphia, 1994.
- [19] R. Etienne-Cummings, S. Fernando, J. Van der Spiegel, and P. Mueller, "Real time 2-D analog motion detector VLSI circuit," in *Proc. Int. Joint Conf. Neural Networks*, vol. IV, 1992, pp. 426–431.
- [20] R. Etienne-Cummings, S. Fernando, N. Takahashi, V. Shtonov, J. Van der Spiegel, and P. Mueller, "A new temporal domain optical flow measurement technique for focal plane VLSI implementation," in *Proc. CAMP'93*, M. Bayoumi, L. Davis, and K. Valavanis, Eds. Piscataway, NJ: IEEE Press, 1993, pp. 241–51.
- [21] R. Etienne-Cummings, R. Hathaway, and J. Van der Spiegel, "An accurate and simple CMOS 'one-over' circuit," *Electron. Lett.*, vol. 29, no. 18, pp. 1618–1620, 1993.
- [22] M. Gottardi, "A CMOS/CCD image sensor for 2D real-time motion estimation," *Sensors and Actuators A*, vols. 46–47, pp. 251–256, 1995.
- [23] A. Simoni, G. Torelli, F. Maloberti, A. Sartori, S. Plevridis, and A. Birbas, "A single chip optical sensor with analog memory for motion detection," *IEEE J. Solid-State Circuits*, vol. 30, pp. 800–806, July 1995.
- [24] C.-Y. Wu and C.-F. Chiu, "A new structure for the 2D silicon retina," *IEEE J. Solid-State Circuits*, vol. 30, pp. 890–897, Aug. 1995.
- [25] J. Kramer, R. Sarpeshkar, and C. Koch, "An analog VLSI velocity sensor," in *Proc. Int. Symp. Circuits Syst. ISCAS 95*, Seattle, WA, 1995, pp. 413–416.
- [26] T. Delbruck, "Silicon retina with correlation-based velocity-tuned pixels," *IEEE Trans. Neural Networks*, vol. 4, pp. 529–541, 1993.
- [27] C. Chong, C. Salama, and K. Smith, "Image-motion detection using analog VLSI," *IEEE J. Solid-State Circuits*, vol. 27, pp. 93–96, Jan. 1992.



Ralph Etienne-Cummings (S'93) was born in Victoria, Seychelles. He received the B.Sc. degree in physics in 1988 from Lincoln University, PA, and the M.S.E.E. and Ph.D. degrees in electrical engineering from the University of Pennsylvania in 1991 and 1994, respectively.

Currently, he is an assistant professor of computer engineering with the Southern Illinois University, Carbondale, IL. His research interests include mixed signal VLSI systems, computational sensors, computer vision, and neuromorphic engineering.



Paul Mueller is cofounder and chairman of Corticon, Inc. and a former professor with the University of Pennsylvania. His earlier research in neuroscience includes work on the molecular basis of the nerve impulse and the function of ion channels in nerve membranes and lipid bilayers. He has worked on neural computation and hardware implementation of neural networks since the early 1960's and has built several large scale electronic neural networks. In addition, he has developed computer models for early vision. Most recently, he has been

involved in the development of a general purpose analog neural computer.



Jan Van der Spiegel (S'73-M'79-SM'90) was born in Aalst, Belgium. He received the engineering degree in electromechanical engineering, and the Ph.D. degree in electrical engineering from the Katholieke University of Leuven, Belgium, in 1974 and 1979, respectively.

From 1980 to 1981, he was a post-Doctoral Fellow with the University of Pennsylvania where he became an assistant professor of electrical engineering in 1981. Currently, he is a professor in electrical engineering with the University of

Pennsylvania. He holds the Bicentennial Chair of the Class of 1940, is the Director of the Center for Sensor Technologies, and House Faculty Master of Ware College at the University of Pennsylvania. His research interests are in artificial neural networks, CCD and CMOS sensors, microsensor technology and low noise, low power, and high speed analog integrated circuits. He is the Editor for North and South America of *Sensors and Actuators Journal*, and is on the editorial board of the *International Journal of High Speed Electronics*, and the *Journal of the Brazilian Microelectronics Society*.

Dr. Van der Spiegel is on the Executive and Program Committees of the IEEE International Solid-State Circuits Conference (ISSCC). He has also served on the Program Committee of the IEEE International Electron Device Meeting (IEDM) and the International Conference on Computer Design (ICCD). He received the Presidential Young Investigator Award, the S. R. Warren and the C. & M. Lindback Awards for distinguished teaching. He is a member of the International Neural Network Society, Phi Beta Delta, and Tau Beta Pi.